OncoTargets and Therapy

Dovepress
Taylor & Francis Group

Open Access Full Text Article

ORIGINAL RESEARCH

Aloperine Induces Ferroptosis of Colorectal Cancer Cells via the Nrf2 Pathway

Jun An, Lixuan Tian, Runze Wang, Demiao Ma, Jingxuan Song, Ruihan Yuan, Jingru Wu, Yuxuan Bu, Jianping Wang

Department of Immunology, Basic Medical Institute, Chengde Medical University, Chengde, Hebei, 067000, People's Republic of China

Correspondence: Jianping Wang, Department of Immunology, Basic Medical Institute, Chengde Medical University, Chengde, Hebei, 067000, People's Republic of China, Email wangjianping5102@cdmc.edu.cn

Objective: This study investigated the effects of ALO on apoptosis and ferroptosis in colorectal cancer HCT116 and SW480 cells and the underlying mechanisms.

Methods: Cells were treated with varying ALO concentrations. CCK-8 assay assessed proliferation. Flow cytometry detected apoptosis. Lipid peroxidation was measured by BODIPY 581/591 C11 dye oxidation and TBA method. GSH content was determined by DTNB method. ROS and intracellular iron levels were assessed using fluorescent probes and iron assays. Molecular docking analyzed ALO-Nrf2 binding. Immunofluorescence detected Nrf2 expression. Western blot quantified apoptosis-related proteins (Bax, Bcl-2) and ferroptosis-related proteins (Nrf2, GPX4, xCT, DMT1). Effects of Nrf2 overexpression on ALO-treated cells were observed.

Results: ALO inhibited cell viability and increased apoptosis dose-dependently. It elevated lipid peroxidation and intracellular iron while reducing GSH. Ferroptosis inhibitors DFO and Fer-1 reversed cell death and reduced apoptosis. ALO induced ROS production, upregulated Bax/Caspase3, and downregulated Bcl-2. Molecular docking suggested ALO binds to Nrf2 via hydrogen bonding. Immunofluorescence and Western blot showed ALO suppressed Nrf2, GPX4, xCT, and DMT1 expression concentration-dependently. Nrf2 overexpression significantly attenuated ALO's inhibitory effects on proliferation and its induction of ferroptosis and apoptosis.

Conclusion: ALO suppresses colorectal cancer cell proliferation by inducing apoptosis and ferroptosis via inhibition of the Nrf2 signaling pathway.

Plain Language Summary: Colorectal cancer is a leading global health problem, and new therapeutic strategies are urgently needed. This study investigated the inhibitory effects of ALO on colorectal cancer cells and the underlying molecular mechanisms. We treated two colorectal cancer cell lines (HCT116 and SW480) with different concentrations of ALO. ALO inhibited cancer cell proliferation in a dose-dependent manner by inducing two forms of cell death: apoptosis (programmed cell death) and ferroptosis (iron-dependent cell death). ALO increased reactive oxygen species (ROS) and lipid peroxidation, reduced the antioxidant GSH level, and elevated intracellular iron content. At the molecular level, ALO binds to and inhibits the key protein Nrf2, which is critical for cellular stress defense. This inhibition downregulated proteins that protect against ferroptosis. Overexpression of Nrf2 significantly reversed the effects of ALO, confirming its key role in the mechanism. Our findings demonstrate that ALO induces apoptosis and ferroptosis in colorectal cancer cells by suppressing the Nrf2 pathway, suggesting its potential as a promising candidate for colorectal cancer treatment. This study provides a novel strategy for developing more effective anti-cancer therapies.

Keywords: colorectal cancer, ALO, ferroptosis, Nrf2 pathway, molecular docking

Introduction

Colorectal cancer (CRC), one of the world's most prevalent malignancies, ranks third in global cancer incidence. According to 2023 statistics, 20% of new cases in the United States occur in individuals aged 50 or younger, with a notable tendency to present as advanced-stage diseases.[1] Additionally, the anatomical distribution of CRC has shifted: the primary site has transitioned from the right colon to the left colon. While tumor screening demonstrates greater efficacy in preventing left-sided

https://doi.org/10.2147/OTT.S575500
Received: 21 October 2025
Accepted: 4 March 2026
Published: 21 March 2026

Graphical Abstract

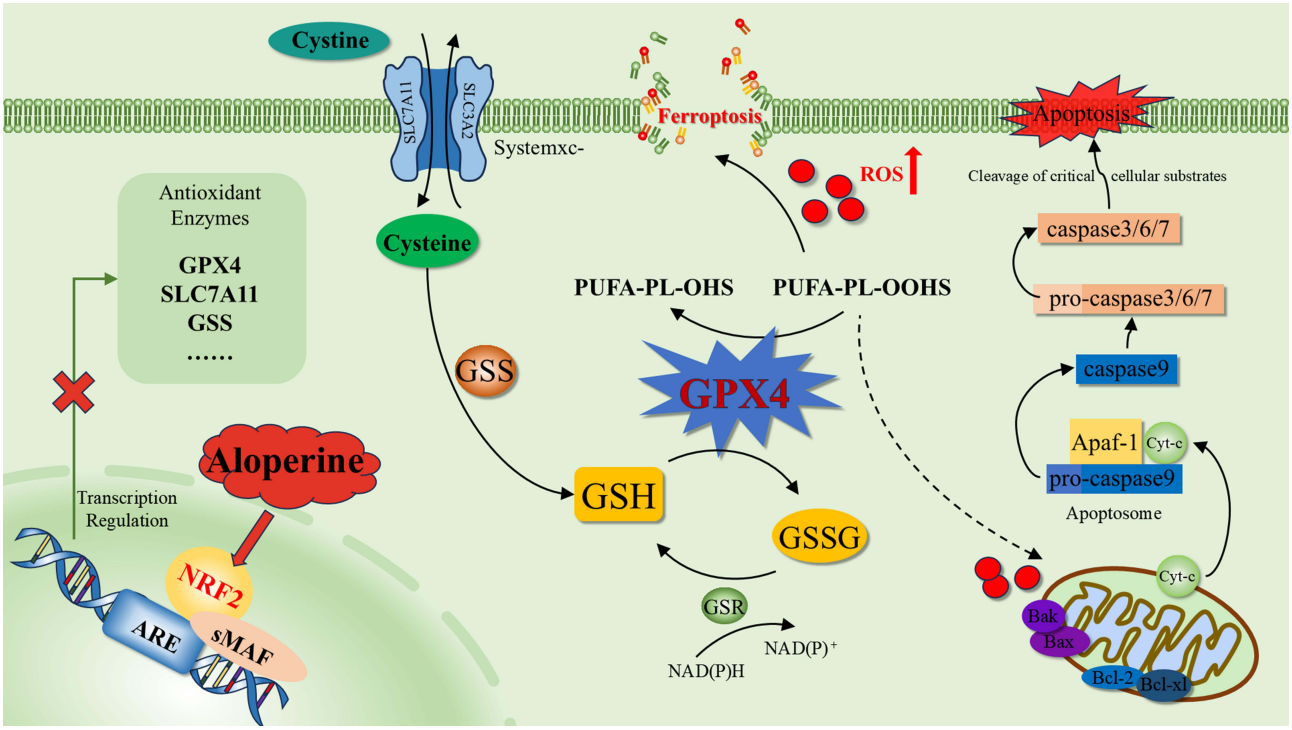

CRC, this phenomenon may reflect underlying changes in disease risk profiles.[2] More than half of the cases can be attributed to modifiable risk factors, such as smoking, unhealthy diet, excessive alcohol consumption, lack of exercise and obesity.[3,4] The treatment methods for CRC include surgical treatment, chemotherapy, radiotherapy, targeted therapy[5,6] and traditional Chinese medicine treatment.[7] Among them, surgical treatment has disadvantages such as greater trauma and a higher risk of complications.[8] Although the combination of postoperative radiotherapy and chemotherapy has effectively improved the survival period of patients,[9] drug resistance remains a major problem in clinical treatment.[10–12] At present, the drugs used in clinical practice to treat CRC also have disadvantages such as high cost, certain toxic and side effects.[13–16] Therefore, seeking safe and effective traditional Chinese medicine can not only reduce treatment costs, but also is of great value in improving the survival period of patients.

Ferroptosis is a distinct form of regulated cell death characterized by iron-dependent phospholipid peroxidation, which is marked by elevated intracellular iron levels and reactive oxygen species (ROS) accumulation.[17] Lipid peroxidation serves as a hallmark of ferroptosis, while abnormal iron metabolism represents a critical regulatory node in its execution pathway.[18,19] Emerging evidence has demonstrated that abnormally increased iron and ROS levels in CRC cells can potently induce ferroptosis. Preclinical studies have further validated that modulating ferroptosis-related signaling pathways effectively suppresses CRC cell progression.

The glutathione peroxidase 4 (GPX4) axis represents one of the canonical ferroptosis regulatory pathways.[20,21] For instance, Zheng[22] et al found that the combined treatment of luteolin and erastin significantly upregulated the expression of HIC1; overexpression of HIC1 significantly enhanced the inhibition of GPX4 expression and promoted ferroptotic cell death. In contrast, silencing of HIC1 weakened the inhibition of GPX4 expression and eliminated ferroptosis. Additionally, Solute Carrier Family 7 Member 11 (xCT) is a factor related to the ferroptosis pathway, which can promote the synthesis of glutathione and reduce the impact of oxidative stress on cells. Mechanistically, Erastin exerts its anti-CRC efficacy by directly targeting xCT, thereby overcoming chemotherapy resistance.[23] These evidences indicate that ferroptosis has broad application prospects in the treatment of CRC. Collectively, these findings highlight the promising therapeutic potential of ferroptosis

modulation in CRC management. The development of safe, effective, and low-toxicity novel agents capable of inducing both ferroptosis and apoptosis in CRC cells holds great promise for providing innovative clinical treatment options and improving patient prognosis.

Sophora alopecuroides L., a species of the genus *Sophora* in the family *Fabaceae*, is predominantly distributed in Inner Mongolia, Xinjiang, Xizang (Tibet) and other regions of China. Its core pharmacological effects include clearing heat, exerting antibacterial and anti-inflammatory activities, relieving pain, exhibiting insecticidal properties and anti-tumor effect.[24] *Alkaloids* are the main active components of *Sophora alopecuroides L*. Aloperine (ALO) is a quinolicidine alkaloid extracted from *Sophora alopecuroides L*.[25] In recent years, there have been a large number of reports on its anti-tumor effect, and the efficacy is well-documented.[26–29] Previous studies have shown that ALO can inhibit tumor proliferation by regulating the JAK-STAT signaling pathway.[30] Yu [31] et al demonstrated that ALO can promote autophagy in tumor cells by inhibiting the Akt/mTOR signaling pathway. Qiu[32] et al found that ALO suppressed migration, invasion, and adhesion in bladder cancer cells by upregulating the expression of TIMP-4. Han[33] et al clarified that miR-296-5p was lowly expressed in CRC cells, and ALO could up-regulate the expression of miR-296-5p and thereby inhibit the expression of STAT3, thereby suppressing the proliferation of CRC cells. However, the effect of ALO on ferroptosis in colorectal cancer cells is currently unclear. This study aims to explore the effects of ALO on the proliferation, apoptosis and ferroptosis of colorectal cancer cells, and further clarify the mechanism by which ALO regulates apoptosis and ferroptosis of CRC cell.

Materials and Methods

Materials

Cell Lines

Human colorectal cancer HCT116 (CL-0096) cell line and SW480 (CL-0223) cell line were purchased from Wuhan Procell Life Science & Technology Co., Ltd. (China).

Drugs

ALO (S2420 purity: 97%), purchased from Selleck Chemicals Company, Deferoxamine mesylate (DFO) (HY-B0988 purity: 99.94%), purchased from MedChemExpress Company, Ferrostatin-1 (Fer-1) (HY-100579 purity: 99.71%), purchased from MedChemExpress Company.

Molecular Docking Technology Website and Software

PDB (https://www.rcsb.org), PubChem (https://pubchem.ncbi.nlm.nih.gov) and CavityPlus (https://www.pkumdl.cn:8000/cavityplus), AutoDOCK Tools (https://autodock.scripps.edu), PyMol (https://www.pymol.org).

Methods

Cell Culture

Colorectal cancer cell lines HCT116 and SW480 were cultured in RPMI-1640 medium supplemented with 10% fetal bovine serum (FBS) (164,210–50, Procell) and 1% penicillin-streptomycin (P1400, Solarbio). The cells were incubated in a constant temperature incubator at 37 °C with 5% CO_2. When the cell confluency reached 70%-80%, the cells were digested with 0.25% trypsin-EDTA and seeded into appropriate culture dishes. On the following day, the cells were treated with ALO at concentrations of 0 μM, 200 μM and 300 μM, followed by an additional 24 hours incubation. The cells were then harvested for subsequent experiments.

CCK-8 Detection

HCT116 cells were seeded in 96-well plate at 4,500 cells/well and SW480 cells at 4,000 cells/well, respectively, with each well containing 100 μL of cell suspension. Five replicate wells were prepared for each treatment group, and a blank group was also set up. Place the culture plate in the incubator for pre-culture (37 °C, 5%CO_2) for 24 hours. Culture media were replaced with fresh media containing ALO at different concentrations (0 μM, 10 μM, 50 μM, 100 μM, 200 μM, 400 μM, 800 μM). After 24 hours of treatment, 10 μL of CCK-8 reagent (K1018-2×5mL, APExBIO) was added to each

well, Place the culture plate in the incubator and continue to culture for 1 hour. Use an enzyme-linked immunosorbent assay (ELISA) reader (ELX808, Berton Instruments, Inc., USA) to measure the absorbance at a wavelength of 450 nm.

Apoptosis Detection

After treating the cells with ALO (0 μM, 200 μM, 300 μM) for 24 hours, the cells were digested with trypsin without EDTA (T1350, Solarbio), collected by centrifugation, resuspended twice in PBS, centrifuged at 4,000×g for 5 minutes, and the supernatant was discarded. The pellet was resuspended thoroughly in 1×binding buffer. Double staining of FITC and PI was performed using the Annexin V-FITC/PI Apoptosis Detection Kit (KGA1107-100, KeyGEN), and the apoptosis rate was detected by flow cytometry (FACSCalibur, Becton, Dickinson and Company, USA). The key parameters for flow cytometry detection were as follows: Gate the target cell population via the FSC/SSC dot plot, with exclusion of cell debris and aggregates; The FL1 channel was used to detect FITC signals and the FL2 channel for PI signals. Dividing the cells into four subpopulations: viable cells (Annexin V^-/PI^-), early apoptotic cells (Annexin V^+/PI^-), late apoptotic cells (Annexin V^+/PI^+), and necrotic cells (Annexin V^-/PI^+). The total apoptotic rate was calculated as the sum of the proportions of early and late apoptotic cells. Single-stain controls (Annexin V-FITC, PI) and unstained cell controls were established for correction of fluorescence spectral overlap between FL1 and FL2 channels, guaranteeing accurate signal detection. 10,000 cells within the gated cell population were collected for each sample. The experimental results were expressed as the percentage of positive cells in each cell subpopulation.

Lipid Peroxidation Measurement

HCT116 and SW480 cells were seeded in 24-well plate containing coverslips and cultured at 37 °C with 5% CO_2 until reaching 50%-70% confluency. Subsequently, cells were treated with ALO at concentrations of 200 μM and 300 μM, with an untreated group set as the control. After 24 hours of treatment, lipid peroxidation sensor BODIPY^{TM} 581/591 C11 (D3861, ThermoFisher) dye stock solution was diluted to a working concentration of 20 μM with serum-free medium, and 500 μL of the probe working solution was added to each well to completely cover the coverslips. The cells were then incubated at 37 °C with 5% CO_2 for 30 minutes in the dark. The probe working solution was discarded, and the cells were washed three times with pre-warmed PBS for 5 minutes each to remove uninternalized probes. Coverslips were mounted with an anti-fluorescence quenching agent, and images were immediately acquired using a laser scanning confocal microscope (FV3000, Olympus Corporation, Japan). Separate channels were set to detect the oxidized form of the C11 probe (excitation/emission: 488/510 nm) and the non-oxidized form (excitation/emission: 581/591 nm). Experimental results were analyzed using ImageJ software.

Detection of MDA by Thiobarbituric Acid (TBA) Method

After treating the cells with ALO (0 μM, 200 μM, 300 μM) for 24 hours, discarded the cell culture supernatant, scraped off the cells with a cell scraper, transferred the cells to an EP tube with a pipette, add 0.5 mL of extract, mixed well for 2 minutes, ultrasonically broke the cells to form a suspension, and determined the protein concentration by the BCA method. Added the reagents one by one in accordance with the instructions of the Cell Malondialdehyde Determination Kit (A003-4-1, Nanjing Jiancheng Institute of Bioengineering). Soaked in water at 95 °C for 80 minutes. After cooling, centrifuged at 4,000×g for 10 minutes. Took 250 μL of each sample of the supernatant into a 96-well plate. Measured the absorbance of each well at 532 nm with an enzyme-linked immunosorbent assay. The MDA content of each sample was subsequently calculated based on the measured absorbance values (A) and quantified protein concentrations (C_{pr}).

$$MDA \text{ content } (\text{nmol/mgprot}) = \frac{A_{sample} - A_{blank}}{A_{standard} - A_{blank}} \times C_{standard} \times C_{pr}$$

Method for Determining Iron Content in Cells

After 24 hours of ALO (0 μM, 200 μM, 300 μM) treatment as described above, cells were counted, and 1×10^7 cells were collected. 0.5 mL of lysis buffer was added, and the cells were disrupted via ice-bath ultrasonication (power: 200 W, 5 seconds of work /5 seconds off, total duration 5 minutes) to prepare a cell suspension. The suspension was then centrifuged at 10,000×g for 10 minutes at 4 °C, and the supernatant was collected and kept on ice for subsequent assays. The 40 mM standard solution was serially diluted with distilled water to obtain working standards with concentrations of 100 μM, 50 μM, 25 μM, 12.5 μM, 6.25 μM, 3.125 μM, 1.5625 μM and 0.78125 μM, respectively. Samples were added to

1.5 mL centrifuge tubes according to the reaction system table After vigorous vortexing for 5 minutes, the mixture was centrifuged at 12,000×g for 10 minutes at room temperature. 200 μL of the upper inorganic phase was transferred to a 96-well plate, and the absorbance was measured at a wavelength of 593 nm. A standard curve was established using the concentrations and corresponding absorbance values of the standard solutions. We determined the intracellular iron content using a Cell Iron Content Assay Kit (BC5315, Nanjing Jiancheng Institute of Bioengineering) and the sample concentrations (X) were calculated from this standard curve. The protein concentration of the samples (C_{pr}) was determined by the BCA method. Finally, the ferrous ion content was calculated using the corresponding formula. Cell Iron Content Detection Kit (BC5315, Nanjing Jiancheng Institute of Bioengineering.

$$\text{Ferrousion content } (\mu\text{mol/mg prot}) = \frac{x \times 10^{-3} \times V_{\text{extract}}}{C_{\text{pr}} \times V_{\text{extract}}} = \frac{0.001x}{C_{\text{pr}}}$$

Experimental Method for the Determination of Glutathione (GSH) Content

After treating the cells with ALO (0 μM, 200 μM, 300 μM) for 24 hours, the cells were digested and collected. An equal volume of pre-cooled 5% Trichloroacetic acid (TCA) (containing 1 mM EDTA) was added and vortex mixed evenly. Centrifuged at 12,000×g for 15 minutes at 4 °C, and took the supernatant for later use. The intracellular GSH content was detected in accordance with the instructions of the reduced glutathione Assay Kit (Microplate Method) (A006-2-1, Nanjing Jiancheng Institute of Bioengineering). The absorbance at 412 nm was measured by the ELISA reader, and the concentration of GSH in the cell supernatant was calculated based on the standard curve.

Detection of ROS by Fluorescent Probes

After treating the cells with ALO (0 μM, 200 μM, 300 μM) for 24 hours, the cells were digested and collected. They were centrifuged at 800×g for 10 minutes, washed with serum-free medium, and centrifuged at 800×g for 10 minutes. Resuspended the cells with DCFH-DA reagent, stained them at 37 °C in the dark for 2 hours, and mixed the cells every 5 minutes during this period. Centrifuged at 800×g for 10 minutes, and washed the cells twice with serum-free medium. Intracellular ROS levels were measured using the Reactive Oxygen Species Assay Kit (E004-1-1, Nanjing Jiancheng Institute of Bioengineering). DCF fluorescence was detected by flow cytometry.

Western Blotting

Cells were harvested after 24 hours treatment with ALO at different concentrations (0 μM, 200 μM, 300 μM). Cells were lysed using RIPA buffer (RIPA:PMSF=100:1), followed by ultrasonic disruption (power: 200 W, 3 seconds of work /3 seconds off, total duration 2 minutes). The lysate was centrifuged at 12000 rpm and 4 °C for 10 minutes, and the supernatant was collected. Total protein was quantified to a concentration of 2 μg/μL using the BCA Protein Concentration Assay Kit (PC0020, Solarbio). Protein samples were heated at 100 °C for 10 minutes to induce protein denaturation. Then 40 μg of protein was subjected to sodium dodecyl sulfate-polyacrylamide gel electrophoresis (SDS-PAGE) on a 10% separating gel at a constant voltage of 120 V. Subsequently, proteins were transferred onto polyvinylidene fluoride (PVDF) membranes (0.45 μm pore size) under a constant current of 200 mA. The membranes were blocked with 5% non-fat milk powder at room temperature for 2 hours, and then included with diluted primary antibodies (Table 1) at 4 °C overnight. The membranes were incubated with corresponding secondary antibodies (1:5000 dilution) at room temperature for 1 hour and washed. Finally, protein bands were developed using an enhanced chemiluminescence (ECL) substrate on a Tanon-6100 chemiluminescence imaging system, and images were captured for subsequent analysis.

Molecular Docking

The three-dimensional crystal structure of the protein was taken from the PDB database, and the three-dimensional structure of ALO was obtained from the PubChem database (SDF format). First, the small molecule PDB number was entered using the Cavity plus website to predict the protein docking active pocket site, and the protein and ligand molecules were processed using AutoDock Tools 1.5.7 software, and semi-flexible molecular docking was performed. After docking, the conformation with the lowest binding free energy was screened out, and the docking results were visualized by PyMOL software.

Table 1 Detailed Description of Antibodies

Target Protein	Molecular Weight (kDa)	Dilution Ratio	Source	Catalog Number	Manufacturer
β-Actin	42	1:3000	Rabbit	AC026	ABclonal
Bax	21	1:1000	Rabbit	Ab32503	Abcam
Bcl-2	26	1:1000	Rabbit	Ab32124	Abcam
Total Caspase-3	32,35	1:5000	Rabbit	Ab32351	Abcam
GPX4	20-23	1:1000	Mouse	67763-1-Ig	Proteintech
XCT	35-40	1:500	Rabbit	26864-1-AP	Proteintech
DMT1	60-70	1:1000	Rabbit	20507-1-AP	Proteintech
Nrf2	68,110	1:500	Rabbit	80593-1-RR	Proteintech

Immunofluorescence

HCT116 and SW480 cells were seeded in 24-well plate with coverslips and cultured at 37 °C with 5% CO_2 to 50%-70% confluency, then treated with ALO at 200 μM and 300 μM for further incubation, with a 0 μM ALO group as the control. After 24 hours of drug treatment, 500 μL of 4% paraformaldehyde was added to each well for fixation at room temperature for 15 minutes. The cells were incubated with 0.1% Triton X-100 at room temperature for 10 minutes, followed by blocking with 5% BSA at room temperature for 60 minutes. The coverslips were incubated with Nrf2 primary antibody (1:200 dilution) at 4 °C overnight. On the next day, ABflo® 488-conjugated Goat anti-Rabbit IgG (H+L) fluorescent secondary antibody (1:200 dilution) (AS053, ABclonal) was added and incubated at room temperature for 1 hour in the dark. DAPI solution (C0060, Solarbio) was added dropwise to cover the coverslips and incubated at room temperature for 10 minutes in the dark. After each reagent treatment, the cells were washed three times with PBS for 5 minutes per wash. The coverslips were mounted with an anti-fluorescence quenching agent (S2100, Solarbio) and observed under a laser scanning confocal microscope. Images were acquired at the excitation/emission wavelength of 488/510 nm, and the fluorescence intensity and intracellular distribution of Nrf2 protein were analyzed. Experimental results were analyzed using ImageJ software.

Plasmid Transfection

Prepare for plasmid transfection when the density of HCT116 and SW480 cells reaches 80%, Tube 1 was prepared by mixing 125 μL Opti-MEM (serum-free medium) with 10 μL Lipofectamine 3000. Tube 2 was prepared by mixing 125 μL Opti-MEM with 2.5 μg DNA plasmids and 5 μL P3000. Combine the solutions from Tube 1 and Tube 2, and incubate the resultant mixture at room temperature for 15 minutes. Supplement the transfection complex with culture medium to a final volume of 2 mL, then add the mixture to the 6-well plate. The empty vector (mock) was transfected simultaneously into the cells as a negative control. Replace the culture medium 48 hours post-transfection, and subject the cells to selection using G418 at concentrations of 600 μg/mL (HCT116 cells) and 400 μg/mL (SW480 cells).

Quantitative Reverse Transcription Polymerase Chain Reaction (qRT-PCR)

Total RNA was extracted using the Trizol reagent. The purity and concentration of RNA were detected using a NanoDrop spectrophotometer (K5600, KAIAO, China), RNA samples with an ratio of 1.8–2.0 were deemed quantified for further experiments. RNA was reverse-transcribed into cDNA using a reverse transcription kit containing gDNA Eraser (for removing genomic DNA). qRT-PCR was then carried out using the SYBR Green l fluorescence dye method for target gene (100ng) amplification. Primer sequences for target genes were as follows: GAPDH (internal control): Forward: 5′-GCACCGTCAAGGCTGAGAAC-3′, Reverse: 5′-TGGTGAAGACGCCAGTGGA-3′. Nrf2: Forward: 5′-GTCACAT CGAGAGCCCAGTC-3′, Reverse: 5′-AGCTCCTCCCAAACTTGCTC-3′. Reactions were cycled under standard conditions (95 °C for 30 seconds, followed by 40 cycles of 95 °C for 5 seconds and 60 °C for 30 seconds). Relative gene expression was calculated using the $2^{-\Delta\Delta Ct}$ method,[34] normalized to GAPDH.

Statistical Processing

Data were analyzed using GraphPad Prism 8.0 (GraphPad Software, Inc). Normality of distributions was verified prior to statistical testing. For comparisons between two groups, unpaired Student's t-tests were performed. For multi-group analyses, one-way analysis of variance (ANOVA) was used to assess significant differences, followed by Tukey's post-hoc test for multiple pairwise comparisons. Statistical significance was defined as $P < 0.05$. All experiments were performed independently in at least three biological replicates, and data are presented as mean ± standard deviation (SD).

Result

ALO Induces Proliferation Inhibition and Apoptosis in CRC Cells

We used CCK-8 to detect the effects of ALO on cell proliferation. Compared with the control group (0 μM), HCT116 and SW480 cells treated with different concentrations of ALO showed significantly reduced cell proliferation in a concentration-dependent manner (Figure 1A, $P < 0.05$). Finally, we chose 200 μM and 300 μM ALO concentrations for the subsequent experiments. The apoptosis detection results showed that compared with the control group (0 μM), the apoptosis rates significantly increased in HCT116 and SW480 cells treated with 200 μM and 300 μM ALO. Moreover, the apoptotic rate of 300 μM ALO increased more significantly (Figure 1B and C, $P < 0.05$).

ALO Induces Ferroptosis in CRC Cells

To observe the effect of ALO on ferroptosis in CRC cells, after treating the HCT116 and SW480 cells with 0 μM, 200 μM and 300 μM for 24 hours, the lipid peroxidation sensor BODIPY 581/591 C11 dye was employed to further detect the Lipid peroxidation levels. The results showed that compared with the 0 μM group, green fluorescence was significantly enhanced and red fluorescence was attenuated after treatment with 200 μM and 300 μM ALO, demonstrating an increase in ROS expression levels (Figure 2A–D, $P < 0.05$). Meanwhile, we detected the MDA, iron content and GSH of the cells. Compared with the control group (0 μM), the levels of MDA and iron content in cells treated with 200 μM and 300 μM ALO significantly increased (Figure 2E–H, $P < 0.05$), and the content of GSH significantly decreased (Figure 2I and J, $P < 0.05$).

Iron Death Inhibitors DFO and Fer-1 Reverse ALO-Induced Ferroptosis

Cell proliferation was detected using the CCK-8 assay in HCT116 and SW480 cells treated with ALO (300 μM) alone or in combination with the iron death inhibitors DFO (20 μM) and Fer-1 (10 μM). The results showed that cell viability was significantly improved in the groups co-treated with ALO plus DFO or Fer-1 compared with the group treated with ALO alone (Figure 3A and B, $P < 0.05$). After 24 hours of co-treatment with ALO and iron death inhibitors (DFO or Fer-1) in HCT116 and SW480 cells, cell apoptosis was analyzed by flow cytometry. The results demonstrated that the apoptotic rate was significantly reduced in the co-treatment groups compared with the ALO alone treatment group (Figure 3C–F, $P < 0.05$).

ALO Induces Mitochondrial Apoptosis in CRC Cells

Lipid peroxidation caused by ferroptosis generates a large amount of ROS to induce mitochondrial apoptosis in cells. Therefore, we detected the intracellular ROS level and the expression of mitochondrial apoptotic proteins. The ROS levels of HCT116 and SW480 cells were detected by flow cytometry. The results showed that compared with the 0 μM group, the ROS expression levels in HCT116 and SW480 cells in the 200 μM and 300 μM groups were significantly enhanced (Figure 4A–D, $P < 0.05$). Western blotting was used to detect the expression of anti-apoptotic protein Bcl-2 and pro-apoptotic proteins (Bax and Caspase3). In HCT116 and SW480 cells, 200 μM and 300 μM ALO treatments led to a significant increase in the ratio of Bax/Bcl-2. Meanwhile, the protein expression level of Caspase3 increased significantly (Figure 4E–J, $P < 0.05$).

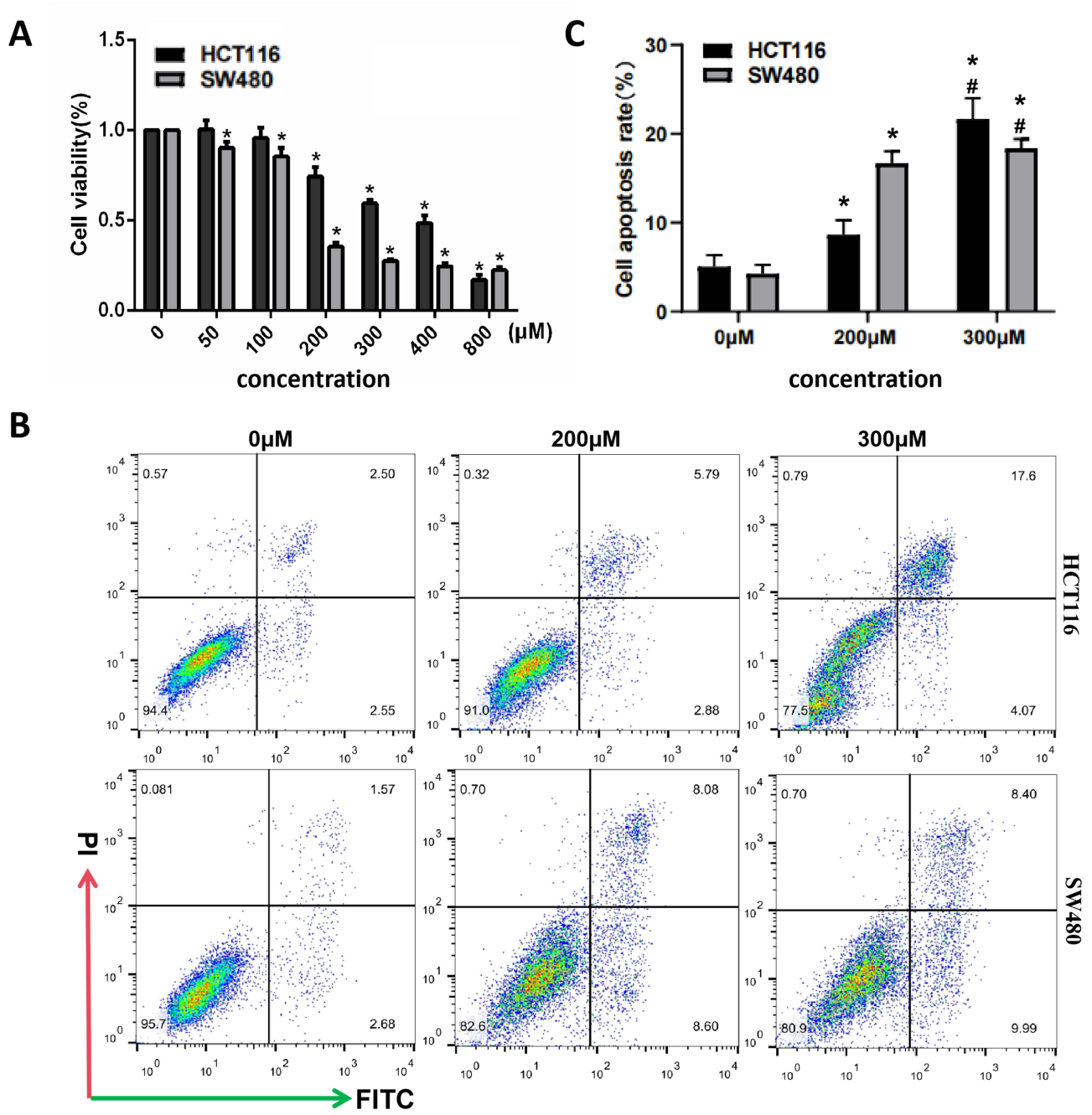

Figure 1 ALO induced inhibition of CRC cell proliferation and apoptosis After treating HCT116 and SW480 cells with different concentrations of ALO for 24 hours, cell viability (**A**) was detected by CCK-8; After HCT116 and SW480 cells were treated with 0 μM, 200 μM and 300 μM ALO for 24 hours, apoptosis (**B** and **C**) was detected by double staining with FITC and PI.The data were expressed as mean ± SD (n = 3). $^{*}p < 0.05$, compared with the control group (0 μM); $^{\#}p < 0.05$, compared with the 200 μM treatment group.

ALO Induces Ferroptosis in CRC Cells by Inhibiting the Nrf2 Pathway

The analysis confirmed the preferred 3D protein structure of the ALO target molecule (Nrf2:2FLU). The molecular docking of ALO and Nrf2 protein showed that the small molecule of the protein showed a high degree of compatibility with the receptor-binding pocket and had hydrogen bonds under natural conditions (Figure 5A). The group with the minimum binding energy of −8.7 kcal/mol was selected as the most favorable conformation of the two binding (Table 2), and the pKd/pKi was calculated to be 6.524 pKd/pKi. Cavity plus evaluated possible active pockets of ALO in Nrf2, and natural ligands could dock to the GLY364-ALA670 domain of the same Nrf2, which was the active binding pocket of

https://doi.org/10.2147/OTT.S575500

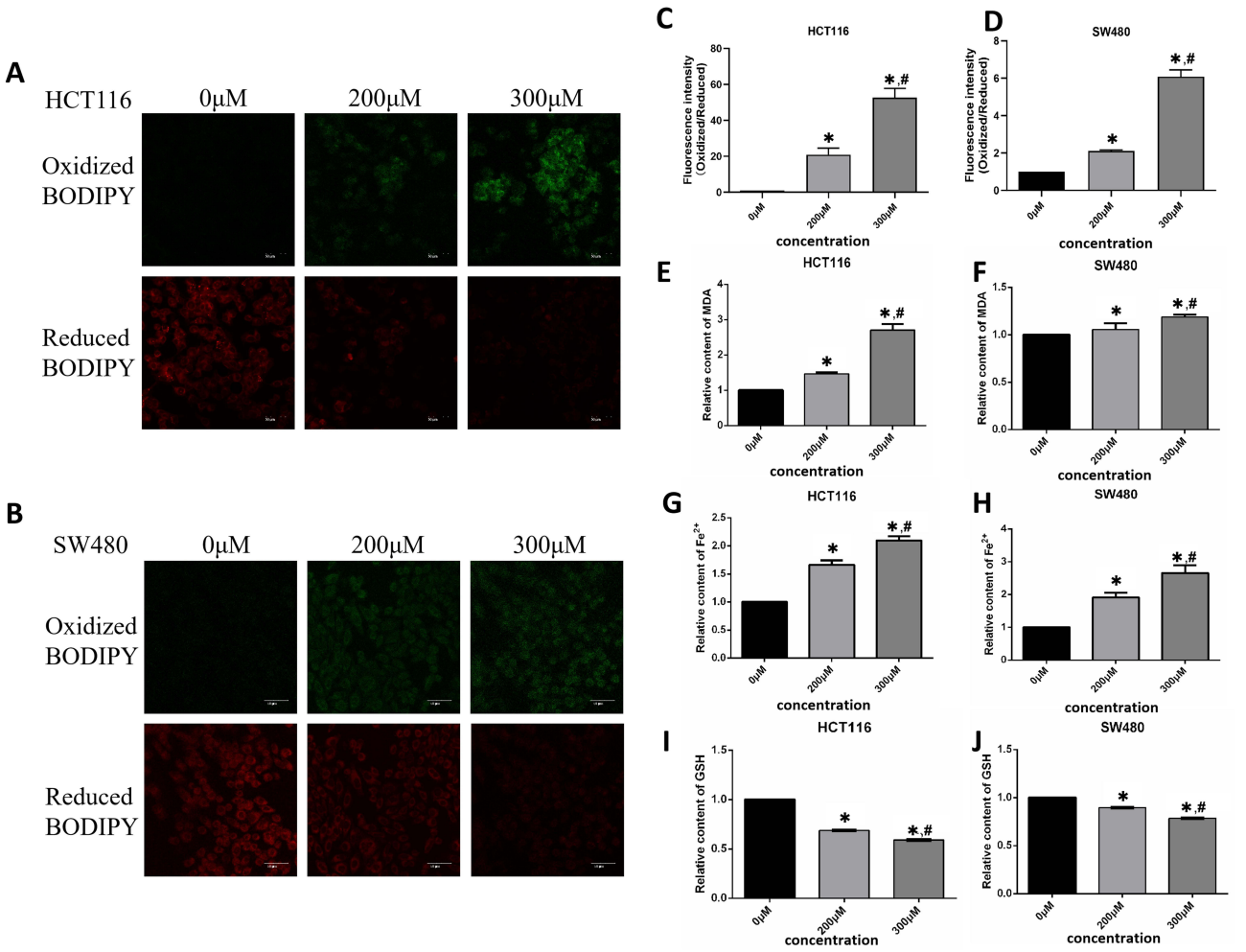

Figure 2 ALO induced ferroptosis in CRC cells After treatment with 0 μM, 200 μM and 300 μM ALO for 24 hours, the lipid peroxidation levels in HCT116 (**A**) and SW480 (**B**) cells were detected by the BODIPY C11 fluorescent probe. (**C** and **D**) Present the quantitative analysis of the corresponding fluorescence intensity ratios. (**E** and **F**) show the relative MDA contents in HCT116 and SW480 cells, respectively. (**G** and **H**) indicate the ferrous ion (Fe^{2+}) contents in HCT116 and SW480 cells, respectively. (**I** and **J**) display the GSH contents in HCT116 and SW480 cells, respectively. The data were expressed as mean ± SD (n = 3). $^{*}p < 0.05$, compared with the control group (0 μM); $^{\#}p < 0.05$, compared with the 200 μM treatment group.

Nrf2 proteins (Figure 5B), including the amino acids ALA-510, GLY-367, LEU-365, VAL-463, ILE-416, GLY-462, LEU-557. These data indicate that ALO has a good affinity for the Nrf2 protein, which occurs by forming an intermolecular force between its polar part and the conserved amino acid residue. Meanwhile, immunofluorescence assay detected Nrf2 expression levels. Compared with the 0 μM group, in HCT116 cells, treatment with 200 μM and 300 μM ALO significantly downregulated Nrf2 expression in a concentration-dependent manner; in SW480 cells, the same concentrations of ALO also markedly reduced Nrf2 expression, with no concentration dependence observed (Figure 5C–F, $P < 0.05$). Nrf2, as an important regulatory factor of ferroptosis, can inhibit ferroptosis by regulating the transcription and translation of DMT1, xCT and GPX4. Furthermore, Western Blotting analysis revealed the protein expression of Nrf2, DMT1, xCT and GPX4. In HCT116 cells, 200 and 300 μM ALO reduced the expression of these four proteins in a concentration-dependent manner (Figure 5G and H, $P < 0.05$). In SW480 cells, the same ALO concentrations decreased Nrf2, DMT1 and GPX4 expression in a concentration-dependent way, whereas xCT expression was inhibited with no concentration dependence (Figure 5I and J, $P < 0.05$).

https://doi.org/10.2147/OTT.S575500

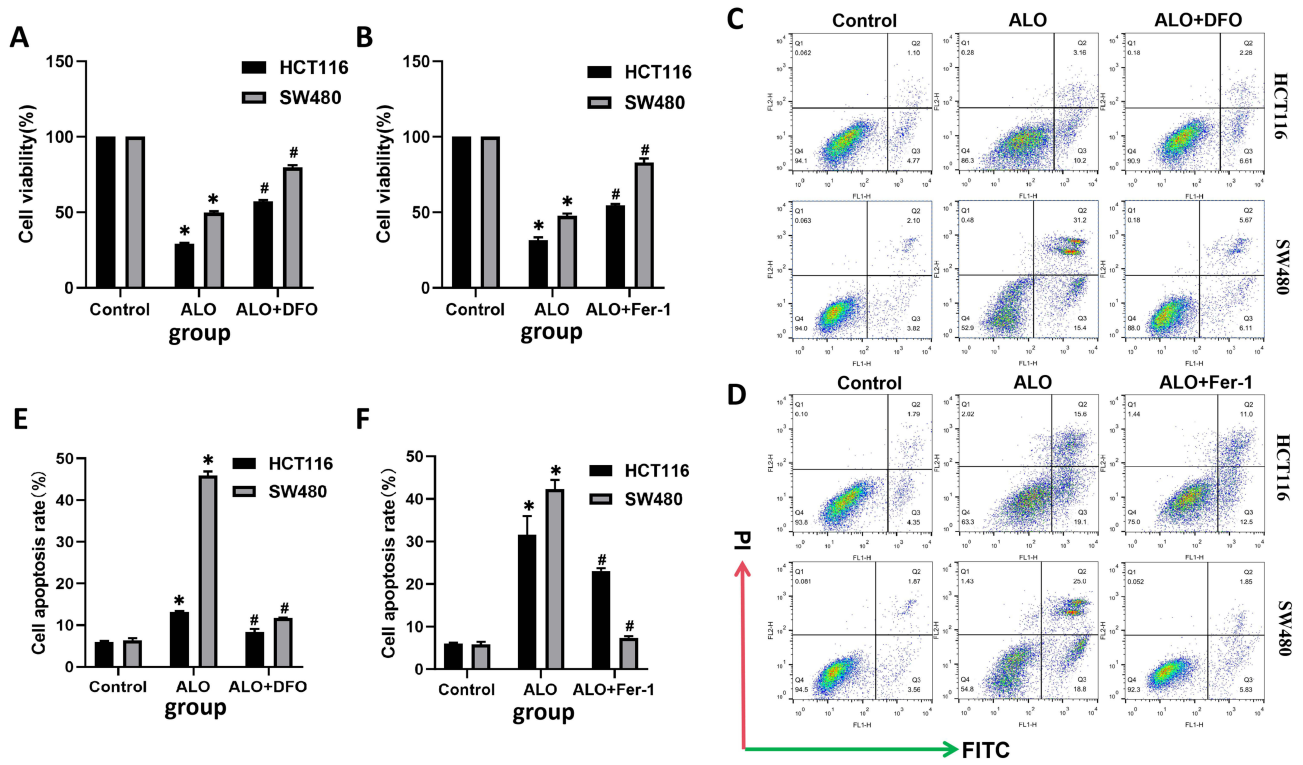

Figure 3 Iron Death Inhibitors DFO and Fer-1 reverse ALO-induced Ferroptosis After treating HCT116 and SW480 cells with DFO and Fer-1.Cell viability of HCT116 (**A**) and SW480 (**B**) cells in different groups was detected by CCK-8. Cell apoptosis changes in DFO (**C**) and Fer-1 (**D**) groups were detected by flow cytometry. (**E** and **F**) show the quantitative statistics of flow cytometry results. The data were expressed as mean ± SD (n = 3). *$p < 0.05$, compared with the control group; #$p < 0.05$, compared with the ALO-treated group.

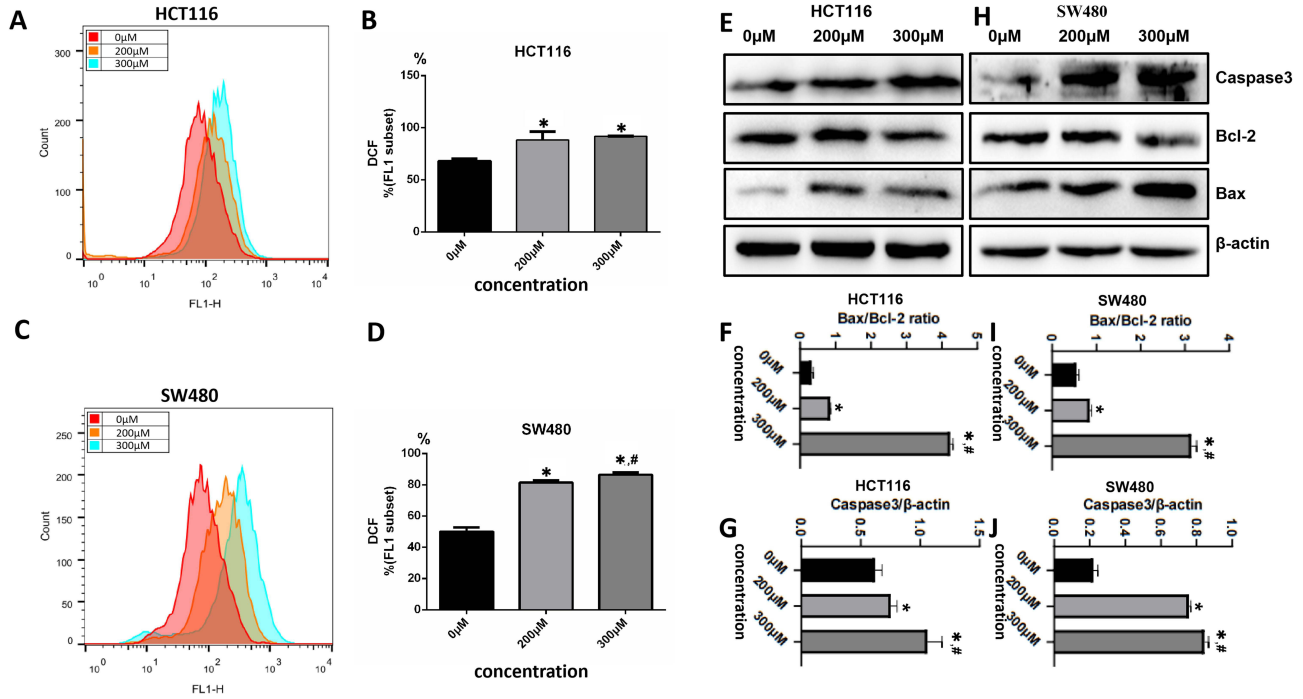

Figure 4 ALO induces mitochondrial apoptosis in CRC cells After treating HCT116 and SW480 cells with different concentrations of ALO (0 μM, 200 μM and 300 μM) for 24 hours, the ROS levels of the cells (**A**–**D**) were detected by flow cytometry. Western blotting was used to detect the protein expressions of Bcl-2, Bax and Caspase3 (**E**–**J**). The data were expressed as mean ± SD (n = 3). *$p < 0.05$, compared with the control group (0 μM); #$p < 0.05$, compared with the 200 μM treatment group.

https://doi.org/10.2147/OTT.S575500

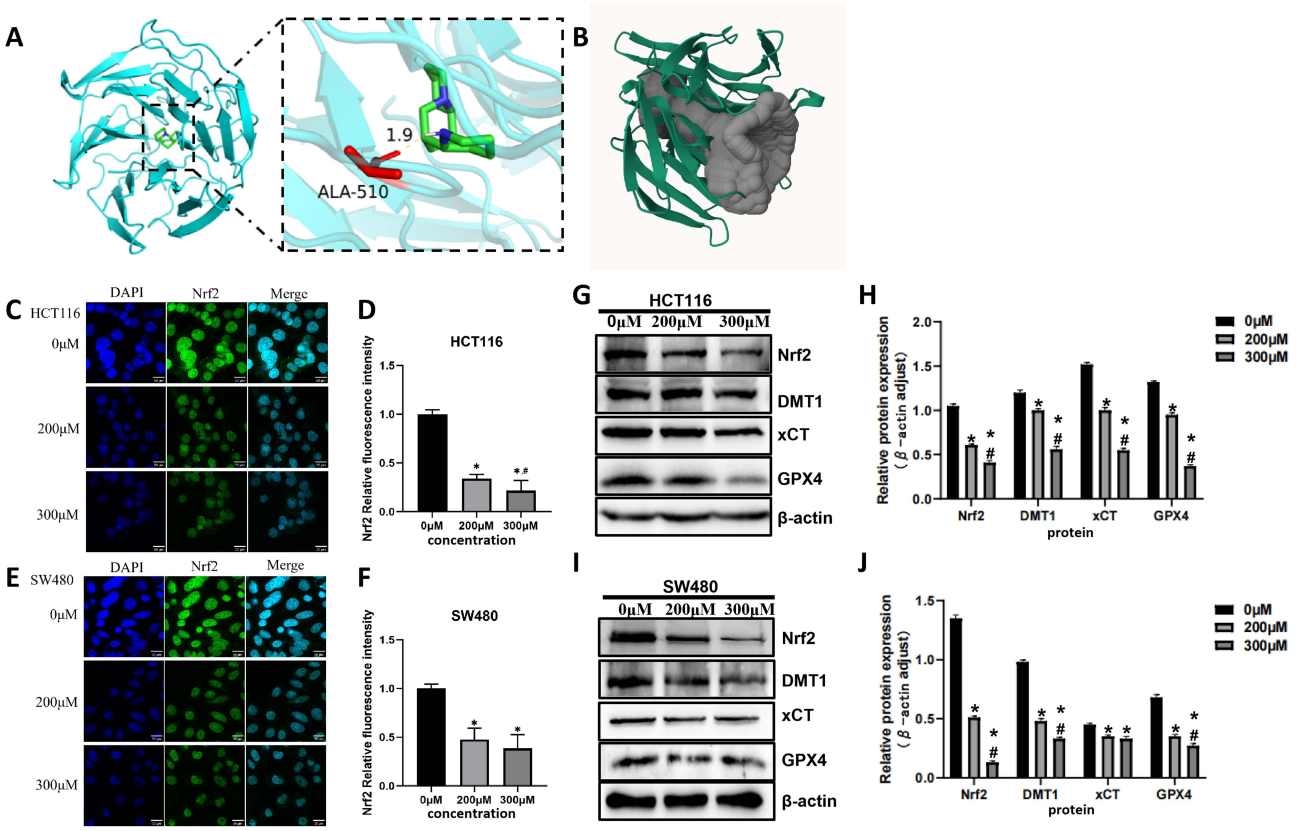

Figure 5 ALO induces ferroptosis in CRC cells by inhibiting the Nrf2 pathway The binding conformation between ALO and the Nrf2 receptor was analyzed using AutoDock Tools. The lowest binding energy conformation was identified at the ALA-510 binding site, which interacts via a hydrogen bond with a length of 1.9 (**A**). Potential active pockets of ALO in the Nrf2 protein were evaluated using CavityPlus software; the GLY364-ALA670 domain was identified as the active binding pocket of Nrf2, and ALO bound to this pocket as expected (**B**). After treating HCT116 and SW480 cells with ALO (0 μM, 200 μM and 300 μM) for 24 hours, immunofluorescence was used to detect intracellular Nrf2 changes in HCT116 (**C** and **D**) and SW480 (**E** and **F**) cells treated with different concentrations of ALO. Western Blotting was used to detect the protein expression levels of Nrf2, DMT1, xCT and GPX4 (**G**–**J**). The data were expressed as mean ± SD (n = 3). $^{*}p < 0.05$, compared with the control group (0 μM); $^{\#}p < 0.05$, compared with the 200 μM treatment group.

Overexpression of Nrf2 Inhibits ALO-Induced Ferroptosis

To investigate the effect of Nrf2 on ALO-induced ferroptosis, we overexpressed Nrf2 in SW480 cells. The results showed that in the cells overexpressing Nrf2, the expression levels of Nrf2 mRNA and protein were significantly increased

Table 2 Nine Different Conformations of ALO and Nrf2 Binding Were Obtained by Autodock Tools

Mode	Affinity (kcal/mol)	Msd l.b	Msd u.b
1	−8.7	0	0
2	−8.4	1.808	2.809
3	−8.2	2.018	5.776
4	−8	1.759	2.954
5	−7.7	3.988	6.485
6	−7.4	4.13	6.938
7	−7.4	3.944	6.518
8	−7.4	4.077	7.898
9	−6.9	6.153	10.145

Note: In this context, msd refers to the maximum spatial distance, where l.b. stands for lower bound and u.b. for upper bound.

https://doi.org/10.2147/OTT.S575500

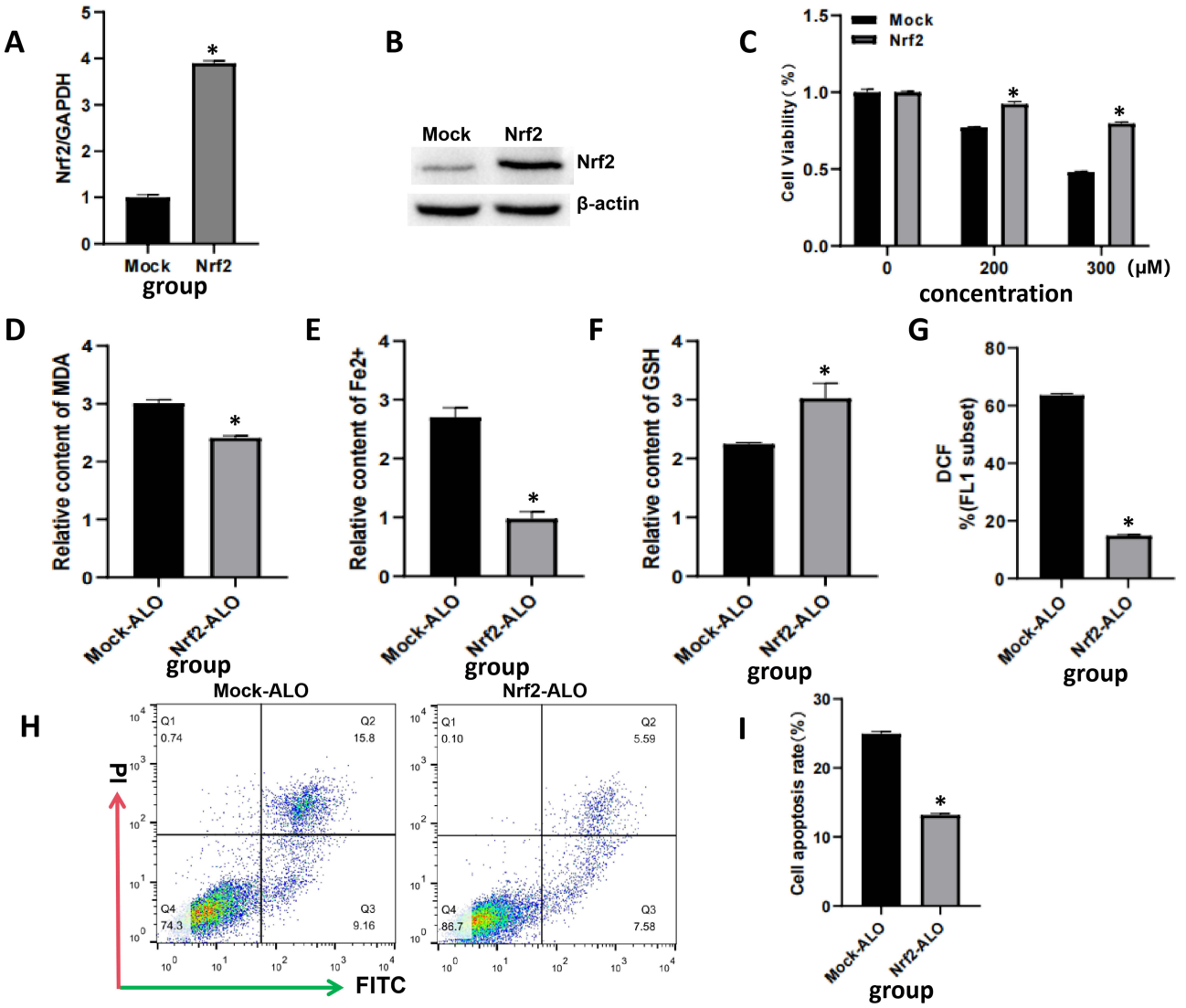

Figure 6 Overexpression of Nrf2 inhibits ALO-induced ferroptosis HCT116 and SW480 cells were transfected with pcDNA3.1-Nrf2 plasmid; Nrf2 mRNA expression was detected by qRT-PCR (**A**), and Nrf2 protein expression by Western blotting (**B**). After 24 hours treatment of mock and Nrf2-overexpressing cells with ALO (300 μM), cell viability was measured by CCK-8 (**C**), and intracellular MDA (**D**), iron (**E**), GSH (**F**) levels were detected; intracellular ROS levels were analyzed by flow cytometry (**G**), and cell apoptosis was assessed by FITC-PI double staining (**H** and **I**). The data were expressed as mean ± SD (n = 3). *$p < 0.05$, compared with the mock group.

(Figure 6A and B, $P < 0.05$). After ALO (300 μM) treated the mock and Nrf2 overexpressing cells for 24 hours, the results showed that the viability of Nrf2 overexpressing cells was significantly increased compared with mock (Figure 6C, $P < 0.05$); The lipid peroxidation level and iron content of the cells decreased significantly (Figure 6D and E, $P < 0.05$); Meanwhile, the level of GSH increased significantly (Figure 6F, $P < 0.05$). The ROS production of Nrf2 overexpressing cells treated with ALO decreased (Figure 6G, $P < 0.05$), and the apoptotic level was significantly reduced (Figure 6H and I, $P < 0.05$).

Discussion

CRC, a prevalent malignant tumor of the gastrointestinal tract, ranks as the second leading cause of cancer-related deaths globally.[35] In 2022, global estimates indicated approximately 1.932 million new CRC cases and 935,000 deaths.[36] In the same year, data from the National Cancer Center showed that there were 517,100 new cases of colorectal cancer and 240,000 deaths in China. Among malignant tumors in China, CRC exhibits the second-highest incidence and the fourth-highest mortality.[36] Although the continuous progress of treatment plans and the emergence of new treatment methods have improved

https://doi.org/10.2147/OTT.S575500

the survival rate of CRC patients, the current treatment methods cannot benefit all colorectal cancer patients. Notably, a substantial proportion of CRC patients still face poor prognoses.[37–39] The SW480 and HCT116 human CRC cell lines, renowned for their genetic stability, are widely utilized in physiological and pathological research on CRC. In this study, these cell lines were employed to investigate the effects of ALO on CRC cell apoptosis and ferroptosis, while elucidating the underlying molecular mechanisms. Experimental results demonstrated that ALO significantly inhibited the proliferation of SW480 and HCT116 cells and promoted cellular apoptosis. Mechanistically, ALO induced lipid peroxidation to inhibit key regulatory factors (eg., Nrf2 and GPX4), thereby facilitating ferroptosis in CRC cells.

ALO is a quinolizidine alkaloid extracted from *bitter beans*. In recent years, there have been various reports on its anti-tumor properties, and it has therapeutic effects on multiple tumors such aslung cancer, kidney cancer, bladder cancer, prostate cancer, breast cancer, ovarian cancer, cervical cancer, thyroid cancer, colorectal cancer, and gastric cancer.[29–32,40] Among them, Liu[27] et al found that ALO inhibits the proliferation, migration and invasion of A549 and H1299 cells through the PI3K/Akt signaling pathway and induces cell apoptosis. Guo[41] et al found that ALO inhibits the autophagosome-lysosome fusion of non-small cell lung cancer by interacting with VPS4A, thereby suppressing the proliferation and migration of tumor cells. Furthermore, Zhang[42] et al found that ALO could induce growth arrest and apoptosis of HCT116 cells. Wang[28] et al proved that ALO can induce apoptosis of SW480 and HCT116 cells, but its molecular mechanism remains incompletely elucidated. Other studies have shown that ALO, through the mitochondrial apoptotic pathway, induces cell cycle arrest at the G2/M phase and has a significant inhibitory effect on the proliferation of CRC cells.[43] This study confirmed that ALO could significantly inhibit the proliferation ability of SW480 and HCT116 cells in a dose-dependent manner and induce apoptosis.

Ferroptosis is an iron-dependent programmed cell death, characterized by: rounded cell shape with reduced volume and intact membrane; mitochondrial shrinkage, cristae loss, outer membrane rupture, and matrix densification; mitochondrial respiratory chain dysfunction leading to reduced ATP production, enhanced ROS accumulation, and aggravated lipid peroxidation.[18] Lipid peroxidation is a hallmark of ferroptosis, and abnormal iron metabolism is a key regulatory node in its executive pathway.[13,18] Emerging evidence has demonstrated that abnormally increased iron and ROS levels in CRC cells can potently induce ferroptosis. Preclinical studies have further validated that modulating ferroptosis-related signaling pathways effectively suppresses CRC cell progression.[44] Fu [45] et al found that ATF3 might induce ferroptosis by blocking Nrf2/Keap1/xCT signal transduction and increase the sensitivity of gastric cancer cells to cisplatin. Zheng[46] found that donafenib and GSK-J4 synergistically promote the expression of HMOX1 and increase the intracellular Fe^{2+} level, ultimately leading to ferroptosis in hepatoma cells. Kuang[47] et al found that palmitic acid exerts its anti-cancer properties by activating endoplasmic reticulum stress/endoplasmic reticulum calcium release/cytoplasmic calcium level to regulate transferrin-dependent ferroptosis. Our results showed that ALO increases the intracellular iron content in colorectal cancer cells, promotes lipid peroxidation, and consumes a large amount of intracellular GSH, thereby inducing cell ferroptosis. Our research results indicate that ALO increases the iron content within colorectal cancer cells, promotes lipid peroxidation, and depletes a large amount of intracellular glutathione, thereby inducing ferroptosis in the cells. Additionally, we have discovered that the ferroptosis inhibitor Ferrostatin-1 or the iron chelator DFO can counteract the inhibitory effect and pro-apoptotic action of ALO, suggesting that ferroptosis is the key mechanism by which ALO induces apoptosis in colon cancer cells.

Nrf2, as a core transcription factor against oxidative stress, plays a key role in regulating ferroptosis and lipid peroxidation.[48] The light and heavy chains (FTL/FTH1) of ferritin and iron transporter (SLC40A1) play key roles in iron metabolism, and they are all regulated by the transcription factor Nrf2.[49,50] Nrf2 also regulates enzymes involved in glutathione synthesis and metabolism, including the catalytic subunit (GCLC) and regulatory subunit (GCLM) of glutamate-cysteine ligase, glutathione synthase (GSS), and the subunit of cystine/glutamate transporter xCT.[51–55] GPX4 is not only a potent iron-lowering agent against lipid peroxides but also an identified transcriptional target of Nrf2.[56–58] Nrf2 is a core regulator of cellular stress defense and cell death pathways. It can inhibit ferroptosis and bidirectionally regulate apoptosis. In cancer therapy, inhibiting Nrf2 can simultaneously enhance the sensitivity of tumor cells to ferroptosis inducers, radiotherapy, and chemotherapy, achieving synergistic killing effects. Thus, it has become an important direction for improving the efficacy of cancer treatment. Our research found that ALO reduced the expression of Nrf2, DMT1, xCT and GPX4 proteins in SW480 and HCT116 cells, significantly decreased intracellular GSH, and

increased intracellular iron and ROS levels. Further molecular docking experiments confirmed that ALO can directly bind to Nrf2 protein, which may directly inhibit the function of Nrf2 and reduce its protein stability. However, this part needs to be further verified. After overexpression of Nrf2 in colorectal cancer cells, the ability of ALO to inhibit proliferation and induce ferroptosis and apoptosis is significantly reduced, indicating that Nrf2 is the core action point of ALO.

At present, there is still a lack of extensive experimental verification regarding the toxicity and side effects of ALO. Based on the results of the CCK-8 assay, we ultimately selected a low dose to determine its anti-tumor effect in order to reduce the impact of its cytotoxicity. Modern research has confirmed that toxic traditional Chinese medicines, especially alkaloid-based ones, exhibit direct tumor-killing effects despite their cytotoxicity; therefore, the development of low-toxicity and high-efficiency anti-tumor drugs is of great importance. Building on existing research, we have clarified the regulatory network of ferroptosis and apoptosis induced by ALO. Studies have demonstrated that ALO may exert a synergistic killing effect by inhibiting the Nrf2 pathway, while increasing the apoptotic rate and inducing ferroptosis — this is presumably the key mechanism underlying its effective suppression of CRC cell proliferation. In the future, we will further investigate the crosstalk between ALO, apoptosis, and ferroptosis, verify its appropriate concentration through animal and clinical experiments, and explore more positive roles of ALO in tumor therapy. This study clarified that ALO exerts an anti-colorectal cancer effect by inhibiting the Nrf2 signaling pathway. However, the further regulatory mechanism awaits further research and lacks confirmation from in vivo studies. We will refine it in the next stage of research.

Conclusion

ALO inhibits colorectal cancer cell proliferation and induces ferroptosis and mitochondrial apoptosis by suppressing the Nrf2 signaling pathway.

Abbreviations

ALO, aloperine; FBS, fetal bovine serum; SDS-PAGE, Sodium Dodecyl Sulfate-Polyacrylamide Gel Electrophoresis; ECL, enhanced chemiluminescence; PVDF, polyvinylidene fluoride; DTNB, 5,5'-Dithiobis (2-nitrobenzoic acid); DFO, Deferoxamine mesylate;Fer-1, Ferrostatin-1; TCA, Trichloroacetic acid; ANOVA, Analysis of Variance; ATF3, Activating Transcription Factor 3; Bax, Bcl-2 Associated X Protein; Bcl-2, B-cell lymphoma 2; Caspase-3, Cysteinyl Aspartate-specific Proteinase-3; CCK-8, Cell Counting Kit-8; CRC, Colorectal cancer; DMT1, Divalent Metal Transporter 1; EDTA, Ethylenediaminetetraacetic acid; ELISA, enzyme-linked immunosorbent assay; GCLC, catalytic subunit; GCLM, Glutamate-Cysteine Ligase Modifier; GPX4, glutathione peroxidase 4; GSH, glutathione; GSS, glutathione synthase; HIC1, Hypermethylated in Cancer 1; HMOX1, Heme Oxygenase 1; Nrf2, Nuclear factor erythroid 2-related factor 2; PBS, Phosphate-Buffered Saline; qPCR, quantitative Polymerase Chain Reaction; ROS, reactive oxygen species; STAT3, Signal Transducer and Activator of Transcription 3; TBA, thiobarbituric acid; TBST, Tris-Buffered Saline with 0.1% Tween-20; TIMP-4, Tissue Inhibitor of Metalloproteinases-4; xCT, Solute Carrier Family 7 Member 11; β-Actin, beta-Actin; MDA, Malondialdehyde; FITC, Fluorescein Isothiocyanate; PI, Propidium Iodide; BCA, Bicinchoninic Acid; DCFH-DA, 2',7'-Dichlorodihydrofluorescein Diacetate; DCF, 2',7'-Dichlorofluorescein; WB, Western Blot; SD, Standard Deviation; ATP, Adenosine Triphosphate; Keap1, Kelch-Like ECH-Associated Protein 1; FTL, Ferritin Light Chain; FTH1, Ferritin Heavy Chain 1; SLC40A1, Solute Carrier Family 40 Member 1; GAPDH, Glyceraldehyde-3-Phosphate Dehydrogenase.

Data Sharing Statement

The datasets used and/or analyzed during the current study are available from the corresponding author upon reasonable request.

Acknowledgments

We would like to thank Elixigen (service@elixigen.com) for English language editing.

Author Contributions

All authors made a significant contribution to the work reported, whether that is in the conception, study design, execution, acquisition of data, analysis and interpretation, or in all these areas; took part in drafting, revising or critically reviewing the article; gave final approval of the version to be published; have agreed on the journal to which the article has been submitted; and agree to be accountable for all aspects of the work.

Funding

This study was funded by Project of Population and Family Planning Commission of Hebei Province, China (Project No. 20160009), Basic Scientific Research Business Expenses of Chengde Medical University (Project No. KY2021024), College Student Innovation and Entrepreneurship Training Program Project of Chengde Medical University (Project No. 2024040), Emphasis Project of Education Department of Hebei Province (ZD2022096).

Disclosure

The authors report no conflicts of interest in this work.

References

1. Siegel RL, Wagle NS, Cercek A, Smith RA, Jemal A. Colorectal cancer statistics, 2023. *CA Cancer J Clin*. 2023;73(3):233–254. doi:10.3322/caac.21772
2. Chen R, Aschmann HE, Chen YH, et al. Racial and ethnic disparities in estimated excess mortality from external causes in the us, march to december 2020. *JAMA Intern Med*. 2022;182(7):776–778. doi:10.1001/jamainternmed.2022.1461
3. Ionescu VA, Gheorghe G, Bacalbasa N, Chiotoroiu AL, Diaconu C. Colorectal cancer: from risk factors to oncogenesis. *Medicina*. 2023;59(9):1646. doi:10.3390/medicina59091646
4. Patel SG, Karlitz JJ, Yen T, Lieu CH, Boland CR. The rising tide of early-onset colorectal cancer: a comprehensive review of epidemiology, clinical features, biology, risk factors, prevention, and early detection. *Lancet Gastroenterol Hepatol*. 2022;7(3):262–274. doi:10.1016/S2468-1253(21)00426-X
5. Abedizadeh R, Majidi F, Khorasani HR, Abedi H, Sabour D. Colorectal cancer: a comprehensive review of carcinogenesis, diagnosis, and novel strategies for classified treatments. *Cancer Metastasis Rev*. 2024;43(2):729–753. doi:10.1007/s10555-023-10158-3
6. Saha S, Ghosh S, Ghosh S, Nandi S, Nayak A. Unraveling the complexities of colorectal cancer and its promising therapies - An updated review. *Int Immunopharmacol*. 2024;143(Pt 1):113325. doi:10.1016/j.intimp.2024.113325
7. Wang Y, Liu P, Fang Y, et al. The effect of long-term traditional chinese medicine treatment on survival time of colorectal cancer based on propensity score matching: a retrospective cohort study. *Evid Based Complement Alternat Med*. 2020;2020:7023420. doi:10.1155/2020/7023420
8. Pallan A, Dedelaite M, Mirajkar N, Newman PA, Plowright J, Ashraf S. Postoperative complications of colorectal cancer. *Clin Radiol*. 2021;76(12):896–907. doi:10.1016/j.crad.2021.06.002
9. Bahadoer RR, Dijkstra EA, van Etten B, et al. Short-course radiotherapy followed by chemotherapy before total mesorectal excision (TME) versus preoperative chemoradiotherapy, TME, and optional adjuvant chemotherapy in locally advanced rectal cancer (RAPIDO): a randomised, open-label, Phase 3 trial. *Lancet Oncol*. 2021;22(1):29–42. doi:10.1016/S1470-2045(20)30555-6
10. Prager GW, Taieb J, Fakih M, et al. Trifluridine–Tipiracil and bevacizumab in refractory metastatic colorectal cancer. *N Engl J Med*. 2023;388(18):1657–1667. doi:10.1056/NEJMoa2214963
11. Singh M, Morris VK, Bandey IN, Hong DS, Kopetz S. Advancements in combining targeted therapy and immunotherapy for colorectal cancer. *Trends Cancer*. 2024;10(7):598–609. doi:10.1016/j.trecan.2024.05.001
12. Ma S-C, Zhang J-Q, Yan T-H, et al. Novel strategies to reverse chemoresistance in colorectal cancer. *Cancer Med*. 2023;12(10):11073–11096. doi:10.1002/cam4.5594
13. Hua Y, Wang R, Liu Y, et al. Metabolomics analysis reveals characteristic metabolites in different levels of oxaliplatin-induced neurotoxicity. *J Sep Sci*. 2024;47(11):e2400164. doi:10.1002/jssc.202400164
14. Bhimani N, Wong GY, Molloy C, Dieng M, Hugh TJ. Cost of colorectal cancer by treatment type from different health economic perspectives: a systematic review. *Eur J Surg Oncol*. 2022;48(10):2082–2093. doi:10.1016/j.ejso.2022.06.023
15. Hua Y, Lv J, Zhang Y, Ding Y, Chen J. LC-MS-based serum metabolomics analysis and potential biomarkers for oxaliplatin induced neurotoxicity in colorectal cancer. *J Pharm Biomed Anal*. 2025;252:116492. doi:10.1016/j.jpba.2024.116492
16. Bhimani N, Wong GYM, Molloy C, et al. Cost of treating metastatic colorectal cancer: a systematic review. *Public Health*. 2022;211:97–104. doi:10.1016/j.puhe.2022.06.022
17. Wang B, Wang Y, Zhang J, et al. ROS-induced lipid peroxidation modulates cell death outcome: mechanisms behind apoptosis, autophagy, and ferroptosis. *Arch Toxicol*. 2023;97(6):1439–1451. doi:10.1007/s00204-023-03476-6
18. Jiang X, Stockwell BR, Conrad M. Ferroptosis: mechanisms, biology and role in disease. *Nat Rev Mol Cell Biol*. 2021;22(4):266–282. doi:10.1038/s41580-020-00324-8
19. Liang D, Minikes AM, Jiang X. Ferroptosis at the intersection of lipid metabolism and cellular signaling. *Mol Cell*. 2022;82(12):2215–2227. doi:10.1016/j.molcel.2022.03.022
20. Liu Y, Wan Y, Jiang Y, Zhang L, Cheng W. GPX4: the hub of lipid oxidation, ferroptosis, disease and treatment. *Biochim Biophys Acta Rev Cancer*. 2023;1878(3):188890. doi:10.1016/j.bbcan.2023.188890
21. Chen M, Shi Z, Sun Y, Ning H, Gu X, Zhang L. Prospects for anti-tumor mechanism and potential clinical application based on glutathione peroxidase 4 mediated ferroptosis. *Int J Mol Sci*. 2023;24(2):1607. doi:10.3390/ijms24021607

22. Zheng Y, Li L, Chen H, et al. Luteolin exhibits synergistic therapeutic efficacy with erastin to induce ferroptosis in colon cancer cells through the HIC1-mediated inhibition of GPX4 expression. *Free Radic Biol Med*. 2023;208:530–544. doi:10.1016/j.freeradbiomed.2023.09.014
23. Xu X, Zhang X, Wei C, et al. Targeting SLC7A11 specifically suppresses the progression of colorectal cancer stem cells via inducing ferroptosis. *Eur J Pharm Sci*. 2020;152:105450. doi:10.1016/j.ejps.2020.105450
24. Wang R, Deng X, Gao Q, et al. *Sophora alopecuroides* L.: an ethnopharmacological, phytochemical, and pharmacological review. *J Ethnopharmacol*. 2020;248:112172. doi:10.1016/j.jep.2019.112172
25. Hu ZX, Zhang J, Zhang T, et al. Aloperine-type alkaloids with antiviral and antifungal activities from the seeds of *Sophora alopecuroides* L. *J Agric Food Chem*. 2024;72(14):8225–8236. doi:10.1021/acs.jafc.4c00992
26. Qiu M, Liu J, Su Y, Liu J, Wu C, Zhao B. Aloperine induces apoptosis by a reactive oxygen species activation mechanism in human ovarian cancer cells. *Protein Pept Lett*. 2020;27(9):860–869. doi:10.2174/0929866527666200320094313
27. Liu F, Liu T, Li H. Aloperine inhibits the progression of non-small-cell lung cancer through the PI3K/Akt signaling pathway. *Cancer Cell Int*. 2021;21(1):662. doi:10.1186/s12935-021-02361-5
28. Wang H, Yang S, Zhou H, et al. Aloperine executes antitumor effects against multiple myeloma through dual apoptotic mechanisms. *J Hematol Oncol*. 2015;8:26. doi:10.1186/s13045-015-0120-x
29. Zheng H, Zhang A, Li D, et al. Aloperine can reverse the cisplatin resistance of colorectal cancer cells via suppressing the HIF-1α/ERK signaling pathway. *Pharmazie*. 2020;75(11):581–585. doi:10.1691/ph.2020.0672
30. Han W, Kong D, Lu Q, Zhang W, Fan Z. Aloperine inhibits colorectal cancer cell proliferation and metastasis progress via regulating miR-296-5p/STAT3 axis. *Tissue Cell*. 2022;74:101706. doi:10.1016/j.tice.2021.101706
31. Yu HI, Shen HC, Chen SH, et al. Autophagy modulation in human thyroid cancer cells following aloperine treatment. *Int J Mol Sci*. 2019;20(21):5315. doi:10.3390/ijms20215315
32. Qiu M, Yu L, Liang J, Xia J, Wang X, Liu J. Aloperine prevents migration, invasion, and adhesion by upregulating timp-4 in human bladder cancer cells. *Protein Pept Lett*. 2023;30(3):250–259. doi:10.2174/0929866530666230124112754
33. Han W, Kong D, Lu Q, Zhang W, Fan Z. Aloperine inhibits proliferation and promotes apoptosis in colorectal cancer cells by regulating the circNSUN2/miR-296-5p/STAT3 Pathway. *Drug Des Devel Ther*. 2021;15:857–870. doi:10.2147/DDDT.S288473
34. Alghamdi R. Al-zahrani M. CRISPR/Cas9-mediated claudin-2 knockout in HCT116 cells reveals its key role in colorectal cancer progression. *Oncol Lett*. 2025;31(2):1–9. doi:10.3892/ol.2025.15407
35. Baidoun F, Elshiwy K, Elkeraie Y, et al. Colorectal cancer epidemiology: recent trends and impact on outcomes. *Curr Drug Targets*. 2021;22(9):998–1009. doi:10.2174/1389450121999201117115717
36. Zhang X, Yang L, Liu S, et al. Interpretation on the report of global cancer statistics 2022. *Zhonghua Zhong Liu Za Zhi*. 2024;46(7):710–721. doi:10.3760/cma.j.cn112152-20240416-00152
37. Liang C, Ji D, Qin F, Chen G. CAF signature predicts the prognosis of colorectal cancer patients: a retrospective study based on bulk RNA sequencing and single-cell RNA sequencing data. *Medicine*. 2023;102(10):e33149. doi:10.1097/MD.0000000000033149
38. Li J, Liu S, Chen J, et al. Uncovering the underlying mechanism of yuanhuacine against colorectal cancer by transcriptomics and experimental investigations. *Phytomedicine*. 2025;140:156570. doi:10.1016/j.phymed.2025.156570
39. Ping G, Tian Y, Zhou Z. Constructing a Tregs-associated signature to predict the prognosis of colorectal cancer patients: a STROBE-compliant retrospective study. *Medicine*. 2022;101(47):e31382. doi:10.1097/MD.0000000000031382
40. Tahir M, Ali S, Zhang W, Lv B, Qiu W, Wang J. Aloperine: a potent modulator of crucial biological mechanisms in multiple diseases. *Biomedicines*. 2022;10(4):905. doi:10.3390/biomedicines10040905
41. Guo W, Zhou H, Wang J, et al. Aloperine suppresses cancer progression by interacting with VPS4A to inhibit autophagosome-lysosome fusion in NSCLC. *Adv Sci*. 2024;11(31):e2308307. doi:10.1002/advs.202308307
42. Zhang L, Zheng Y, Deng H, Liang L, Peng J. Aloperine induces G2/M phase cell cycle arrest and apoptosis in HCT116 human colon cancer cells. *Int J Mol Med*. 2014;33(6):1613–1620. doi:10.3892/ijmm.2014.1718
43. Liu JS, Huo CY, Cao HH, et al. Aloperine induces apoptosis and G2/M cell cycle arrest in hepatocellular carcinoma cells through the PI3K/Akt signaling pathway. *Phytomedicine*. 2019;61:152843. doi:10.1016/j.phymed.2019.152843
44. Li H, Yu K, Hu H, et al. METTL17 coordinates ferroptosis and tumorigenesis by regulating mitochondrial translation in colorectal cancer. *Redox Biol*. 2024;71:103087. doi:10.1016/j.redox.2024.103087
45. Fu D, Wang C, Yu L, Yu R. Induction of ferroptosis by ATF3 elevation alleviates cisplatin resistance in gastric cancer by restraining Nrf2/Keap1/xCT signaling. *Cell Mol Biol Lett*. 2021;26(1):26. doi:10.1186/s11658-021-00271-y
46. Zheng C, Zhang B, Li Y, et al. Donafenib and GSK-J4 synergistically induce ferroptosis in liver cancer by upregulating HMOX1 expression. *Adv Sci*. 2023;10(22):e2206798. doi:10.1002/advs.202206798
47. Kuang H, Sun X, Liu Y, et al. Palmitic acid-induced ferroptosis via CD36 activates ER stress to break calcium-iron balance in colon cancer cells. *FEBS J*. 2023;290(14):3664–3687. doi:10.1111/febs.16772
48. Hu S, Zou X, Fang Y, Liu C, Chen R, Ji L. Research progress of nrf2 and ferroptosis in tumor drug resistance. *Zhongguo Fei Ai Za Zhi*. 2023;26(10):765–773. doi:10.3779/j.issn.1009-3419.2023.101.31
49. Yan R, Lin B, Jin W, Tang L, Hu S, Cai R. NRF2, a Superstar of Ferroptosis. *Antioxidants*. 2023;12(9):9. doi:10.3390/antiox12091739
50. Zhang L, Zhang J, Jin Y, et al. Nrf2 Is a potential modulator for orchestrating iron homeostasis and redox balance in cancer cells. *Front Cell Dev Biol*. 2021;9:728172. doi:10.3389/fcell.2021.728172
51. Liu J, Huang C, Liu J, et al. Nrf2 and its dependent autophagy activation cooperatively counteract ferroptosis to alleviate acute liver injury. *Pharmacol Res*. 2023;187:106563. doi:10.1016/j.phrs.2022.106563
52. Wen RJ, Dong X, Zhuang HW, et al. Baicalin induces ferroptosis in osteosarcomas through a novel Nrf2/xCT/GPX4 regulatory axis. *Phytomedicine*. 2023;116:154881. doi:10.1016/j.phymed.2023.154881
53. Yang Z, Zou S, Zhang Y, et al. ACTL6A protects gastric cancer cells against ferroptosis through induction of glutathione synthesis. *Nat Commun*. 2023;14(1):4193. doi:10.1038/s41467-023-39901-8
54. Wu R, Chen X, Wu H, et al. Nrf2 activation contributes to hepatic tumor-augmenting effects of developmental arsenic exposure. *Sci Total Environ*. 2022;837:155685. doi:10.1016/j.scitotenv.2022.155685
55. He J, Hewett SJ. Nrf2 regulates basal glutathione production in astrocytes. *Int J Mol Sci*. 2025;26(2):2. doi:10.3390/ijms26020687

56. Wang Y, Yan S, Liu X, et al. PRMT4 promotes ferroptosis to aggravate doxorubicin-induced cardiomyopathy via inhibition of the Nrf2/GPX4 pathway. *Cell Death Differ*. 2022;29(10):1982–1995. doi:10.1038/s41418-022-00990-5
57. Zhang Z, Fu C, Liu J, et al. Hypermethylation of the Nrf2 Promoter Induces Ferroptosis by Inhibiting the Nrf2-GPX4 Axis in COPD. *COPD*. 2021;16:3347–3362. doi:10.2147/COPD.S340113
58. Pu X, Wu H, Liu X, Yang F. PRMT4 Reduced Erastin-Induced Ferroptosis in Nasopharyngeal Carcinoma Cisplatin-Resistant Cells by Nrf2/GPX4 Pathway. *J Environ Pathol Toxicol Oncol*. 2025;44(1):57–71. doi:10.1615/JEnvironPatholToxicolOncol.2024053754